Journal of Computational Physics **160,** 1–28 (2000)
doi:10.1006/jcph.2000.6418, available online at http://www.idealibrary.com on IDEAL®

M-Matrix Flux Splitting for General Full Tensor Discretization Operators on Structured and Unstructured Grids

Michael G. Edwards

Department of Petroleum Engineering, Green Earth Sciences, Stanford University, Stanford, California 94305
E-mail: Medwards@pangea.stanford.edu

Received March 2, 1999; revised November 24, 1999

Diagonal tensor flux approximations are commonly used in fluid dynamics. This approximation introduces an O(1) error in flux whenever the coordinate system is nonaligned with the principal axes of the tensor which is particularly common when employing curvilinear gridding. In general a consistent full tensor flux approximation leads to a significant increase in support and consequent size of the Jacobian matrix. After decomposition of a general full tensor flux into a diagonal tensor flux together with cross terms, time-split semi-implicit, stable, full tensor flux approximations are introduced with in a general finite volume formalism, enabling the standard diagonal tensor Jacobian matrix structure to be retained for single phase flow, IMPES, and standard block fully implicit formulations while ensuring spatial consistency of the discretization for both structured and unstructured grids. Stability of the scheme is proven for constant elliptic coefficients. The results presented demonstrate the benefits of the method for multiphase flow within a fully implicit framework on structured and unstructured grids. © 2000 Academic Press

Key Words: M-matrix; flux continuous; locally conservative; finite volume; anisotropic; tensor; 9 point; discontinuous coefficients; flux splitting; unstructured.

1. INTRODUCTION

Diagonally dominant M-matrices are obtained for the most common and fundamental discrete operators that occur in numerical approximation of partial differential equations. Classical examples result from the use of first-order upwind schemes for hyperbolic systems and standard five-point schemes (in 2-D, 7 in 3-D) that are used for approximation of Laplacian and diagonal tensor diffusion operators; e.g., [1, 2]. Approximation of full tensor operators introduces additional cross terms that cause the support of the scheme (and thus the matrix bandwidth) to be increased while unconditional diagonal dominance is reduced to being at best conditional or completely lost [3].

0021-9991/00 $35.00

Perhaps the most common example of a full tensor in fluid dynamics is due to the use of nonorthogonal and/or unstructured grids, which cause off-diagonal terms to appear in the flow equations. For example, when discretizing systems of equations that describe flow in porous media, which is the main focus of this paper, or incompressible Euler and Navier–Stokes equations, the support of a full tensor pressure equation typically increases above that of the standard scheme on a logical Cartesian grid from 5 to 9 nodes in 2-D and from 7 to 19 or 27 nodes in 3-D, and therefore represents a potentially large increase in computational cost, as the pressure field is recalculated at every time step of the flow calculation.

Full tensor approximation is a particularly important issue for flow in porous media [3–20]. A major assumption in most commercial simulators is that the flux depends on a diagonal tensor and that the consequent discretizations employ minimal five- and seven-node operators. The design and efficiency of such codes are intrinsically linked to the diagonal tensor assumption. However, this assumption is true only if the computational grid is aligned with the principal axes of the tensor.

In general a full tensor arises in reservoir simulation whenever (a) the medium is anisotropic and the local frame of reference is nonaligned with the principal axes [23], (b) nonorthogonal and/or unstructured grids are employed [3–19], and (c) fine scale cross-flow upscaling is performed, particularly for cross-bedding [21]. Consequently all diagonal tensor simulators will suffer from inconsistent O(1) errors in flux [4, 7, 10–12] when applied to cases involving these major features. In particular, while these simulators appear to allow for nonorthogonal grids through the definition of corner point geometry, only the diagonal tensor flux permeability–geometry contribution is included, which leads to an O(1) error in flux (even for Laplaces equation) on a nonorthogonal grid [7].

The focus of this paper is on the development of finite volume schemes that employ spatially consistent full tensor fluxes while retaining standard diagonal tensor matrix or reduced Jacobian matrix inversion.

The flow equations are given in Sections 2 and 3. In Section 4 it is shown that each of the full tensor fluxes as defined by the schemes presented in [3–8, 10–17] in a block-centered, point-distributed, or cellwise constant coefficient finite volume context can be decomposed into a two-point diagonal tensor flux with a coefficient that is defined via a consistent factorization of the scheme together with cross terms. It is also shown that the fluxes of the formulations can be expressed in an analogous discrete form; this observation is exploited in Sections 6 and 7, where the simpler cellwise constant coefficient schemes are used to contrast the effects of matrix splitting and flux splitting on discrete error, conservation, and stability.

The conditions required for a full tensor discretization to generate an M-matrix are summarized in Section 5. Split schemes are first considered at the matrix level in Section 6, and the properties of the resulting preconditioning techniques are noted.

Semi-implicit split fluxes are defined for each type of finite volume scheme in Section 7. The split fluxes are composed of a fully implicit two-point diagonal tensor flux together with explicit cross-flow terms. The resulting split flux generalizes the deferred correction IMPES type schemes of [7] to a *semi-implicit* general scheme framework, enabling full tensor operators to be incorporated in a *standard fully implicit formulation* while retaining the standard block Jacobian two-point flux matrix and thus resulting in gains in efficiency while only requiring minimal code changes. An error analysis demonstrates that semi-implicit flux splitting formally introduces an error of order Δt, which is confirmed in a convergence study. A stability analysis is also presented for the case of the split single-phase

pressure equation and demonstrates unconditional stability for spatially constant elliptic coefficients.

The split flux schemes are extended to triangular grids in Section 8, generalizing the split schemes to both structured and generally unstructured grids composed of quadrilateral and/or triangular grid cells.

The semi-implicit schemes are applied to a number of porous media two phase flow problems in Section 9, involving strong cross flow due to the orientation of the grid relative to the problem; benefits of the method are clearly demonstrated for structured and unstructured grids while the large time step advantages of a fully implicit formulation are maintained.

2. THE FLOW EQUATIONS

Reservoir simulation and (environmental) aquifer remediation involve solving a coupled system of essentially hyperbolic conservation laws (for fluid transport) and an elliptic or parabolic equation for the pressure. The coupling between the equations is via the fluid velocity, which is defined by Darcy's law to be proportional to the pressure gradient.

Without loss of generality in terms of the numerical method's applicability, the schemes presented here are illustrated with respect to simplified two-phase incompressible flow models, with unit porosity, and where gravity, capillary pressure, and diffusion are neglected. The continuity equation for each phase $j = 1, \ldots, N_p$ (here $N_p = 2$) is written as

$$\int_\Omega \left(\frac{\partial s_j}{\partial t} + \nabla \cdot \mathbf{v}_j \right) d\tau = m_j(x, y), \tag{2.1}$$

where the integral is taken over domain Ω and $\nabla = (\partial_x, \partial_y)$. The jth phase saturation s_j is defined by the ratio of phase volume τ_j to pore volume τ_{pv} with $s_j = \tau_j / \tau_{pv}$, and m_j can be a specified phase flux. Since the pore volume must always be filled by the fluids present, this gives rise to the volume balance

$$\sum_{j=1}^{N_p} s_j = 1. \tag{2.2}$$

The momentum equations are defined through Darcy's law, where

$$\mathbf{v}_j = -\lambda_j \mathbf{K} \nabla \Phi \tag{2.3}$$

is the jth phase velocity, $\mathbf{K}$ can be a *full* rock permeability tensor, Φ is the pressure, and the jth phase mobility is given by

$$\lambda_j = k_{rj}(s_j)/\mu_j, \tag{2.4}$$

where μ_j and k_{rj} are the respective phase viscosity and relative permeability. An equation for pressure can be derived by summation of Eq. (2.1) over the phases and using (2.2) to give

$$\int_\Omega (\nabla \cdot \mathbf{V}_T)\, d\tau = \int_\Omega -\nabla \cdot \left(\mathbf{K} \sum_{j=1}^{N_p} \lambda_j \nabla \Phi \right) d\tau = \sum_{j=1}^{N_p} m_j = m(x, y), \tag{2.5}$$

where $\mathbf{V}_T$ is the total sum of phase velocities and m is the net flux. Neumann boundary conditions apply on boundary $\partial\Omega$ and require zero flux on solid walls together with reflection conditions for saturations s. Inflow–outflow conditions apply at wells where fluxes are

prescribed together with Dirichlet conditions for s, and pressure must be specified at least at one point. Initial data in terms of saturation/concentration and pressure fields are also prescribed. Further details can be found in [1].

3. GENERAL ELLIPTIC TENSOR EQUATION

We shall temporarily consider the single-phase pressure equation (variant of Eq. (2.5)) expressed as

$$-\int_{\Omega} \nabla \cdot (\mathbf{K} \nabla \Phi)\, d\tau = m(x, y). \tag{3.1}$$

The matrix $\mathbf{K}$ can be a diagonal or full Cartesian tensor with the general form

$$\mathbf{K} = \begin{pmatrix} K_{\alpha\alpha} & K_{\alpha\beta} \\ K_{\alpha\beta} & K_{\beta\beta} \end{pmatrix}, \tag{3.2}$$

where off-diagonal Cartesian terms can be due to cross-bedding and/or upscaling [21]. The tensor $\mathbf{K}(x, y)$ can be discontinuous across internal boundaries of Ω, and the full tensor pressure equation is assumed to be elliptic such that $K_{\alpha\beta}^2 \leq K_{\alpha\alpha} K_{\beta\beta}$.

In this work the pressure equation is defined in a general curvilinear coordinate system defined with respect to a uniform dimensionless transform space (ξ, η). For an arbitrary control volume Ω_C with boundary $\partial\Omega_C$ and surfaces that are tangential to constant (ξ, η) (replacing Ω with Ω_C), Eq. (3.1) is integrated over Ω_C via the Gauss flux theorem to yield

$$\Delta_\xi F + \Delta_\eta G = m(x, y), \tag{3.3}$$

where $\Delta_\xi F$ and $\Delta_\eta G$ are the respective differences in net flux with respect to (ξ, η). Resolving the components of velocity along the unit normals to the curvilinear coordinates (ξ, η) gives rise to the general tensor flux components

$$F = -\int_{\delta\Omega_C} (T_{aa}\Phi_\xi + T_{ab}\Phi_\eta)\, d\eta, \qquad G = -\int_{\delta\Omega_C} (T_{ab}\Phi_\xi + T_{bb}\Phi_\eta)\, d\xi, \tag{3.4}$$

where the general tensor $\mathbf{T}$ has canonical coefficients defined by

$$\begin{aligned} T_{aa} &= \left(K_{\alpha\alpha} y_\eta^2 + K_{\beta\beta} x_\eta^2 - 2K_{\alpha\beta} x_\eta y_\eta\right)/J \\ T_{bb} &= \left(K_{\alpha\alpha} y_\xi^2 + K_{\beta\beta} x_\xi^2 - 2K_{\alpha\beta} x_\xi y_\xi\right)/J \\ T_{ab} &= \left(K_{\alpha\beta}(x_\xi y_\eta + x_\eta y_\xi) - (K_{\alpha\alpha} y_\xi y_\eta + K_{\beta\beta} x_\xi x_\eta)\right)/J \end{aligned} \tag{3.5}$$

and $J(x, y) = x_\xi y_\eta - x_\eta y_\xi$. Thus any scheme applicable to a full tensor also applies to any curvilinear grid independent of the grid orthogonality. Ellipticity of $\mathbf{T}$ follows from ellipticity of Eq. (3.2), and by Eq. (3.5) even a diagonal anisotropic cartesian tensor also leads to a full tensor on a curvilinear *orthogonal* grid. The general tensor $\mathbf{T}$ expresses a certain duality between the geometry and permeability, with geometry and physical space Cartesian permeability combined into a general tensor that can be viewed as a transformed permeability

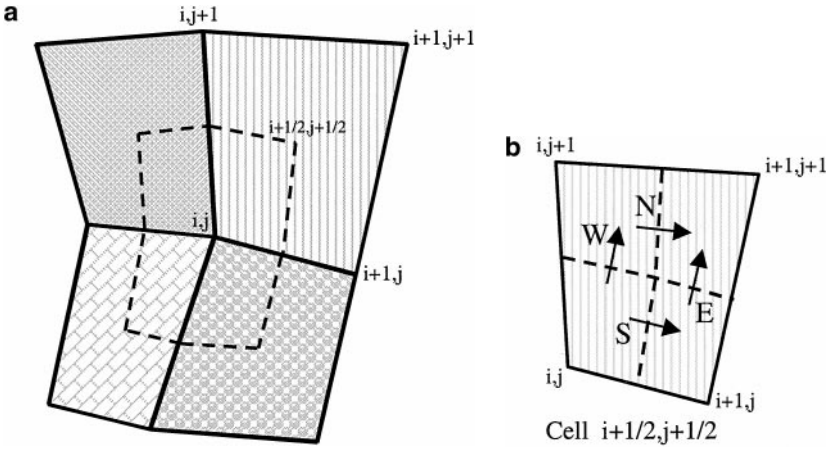

FIG. 1. Dual variable scheme, control volume, and flux calculation. Cell vertex flow variable, cellwise constant tensor (shaded). (a) Dashed line, surface of control volume i, j. (b) Cellwise flux locations N, S, E, W.

with respect to a uniform (Cartesian) grid. For example, upscaling can be performed with respect to the general tensor [16], which shows that geometry and permeability effects can be treated in an equivalent fashion.

4. FINITE VOLUME FORMULATIONS

The finite volume schemes considered in this work are either

(a) dual variable cell vertex based with flow variables located at cell vertices while the rock permeability tensor is piecewise constant over each cell (Fig. 1) or

(b) control-volume distributed such that flow variables and rock properties, e.g., rock permeability tensor, share the same location within the control volume (Fig. 2; the shading indicates constant permeability); this includes both the traditional cell-centered scheme where the control volume is taken to be the grid cell and flow and rock variables are located at the cell center (velocity is cell face centered), and point distributed (i.e., vertex centered)

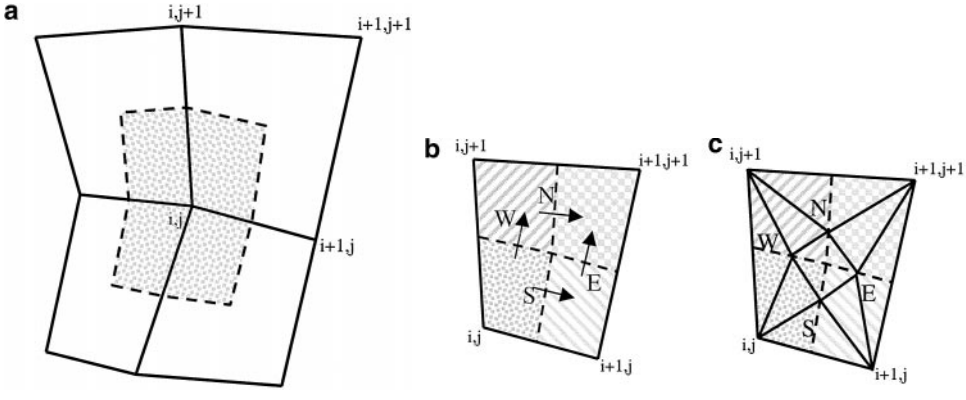

FIG. 2. Control volume distributed scheme, control volume, and flux calculation. Cell vertex flow variable, constant tensor per control volume (shaded). (a) Dashed line, surface of control volume i, j. (b) Cellwise fluxes N, S, E, W. (c) Subcell triangle basis for flux continuity.

such that flow variables and the rock permeability tensor are located at cell vertices and are piecewise constant over each cell vertex control volume.

In this section it is shown that the fluxes resulting from the two formulations can be expressed in an analogous discrete form and that each flux can be decomposed into a leading diagonal tensor two-point operator with a coefficient that is defined via a consistent factorization of the scheme together with cross terms.

While the focus here is on cell vertex/point-distributed schemes, the methods presented have also been developed for cell-centered formulations by translating the operations onto a grid that is essentially the dual mesh.

To fix ideas, finite volume discretizations will be defined with respect to grid vertex control volumes. For vertex i, j the control volume is defined by joining cell centers to the cell edge midpoints of those edges that are attached to the (i, j)th vertex (Figs. 1b and 2b) and as a result, each quadrilateral is subdivided into four quadrants, with each quadrant forming part of the control volume associated with the corresponding cell vertex; consequently, each control volume is generally composed of a polygon.

In the two types of discretization considered, the flow variables are always located at the grid vertices, and the fluxes are assembled in a cellwise fashion. For a given cell, a flux is calculated along the normal to each control volume face inside the cell (Figs. 1b and 2b), leading to the four fluxes

$$F_{N_{i+1/2,j+1/2}}, \qquad F_{S_{i+1/2,j+1/2}}, \qquad F_{E_{i+1/2,j+1/2}}, \qquad F_{W_{i+1/2,j+1/2}} \tag{4.1}$$

per quadrilateral, where suffixes N, S, E, W indicate the north, south, east, and west quadrature locations. The fluxes are distributed to their adjacent cell edges, which are intersected by the control volume faces. In 2-D each cell edge is intersected by one (if a boundary) or two control volume faces. In this way the finite volume scheme is assembled via summation of net edge-based fluxes,

$$F_{i+1/2,j} = F_{N_{i+1/2,j-1/2}} + F_{S_{i+1/2,j+1/2}}, \qquad F_{i,j+1/2} = F_{E_{i-1/2,j+1/2}} + F_{W_{i+1/2,j+1/2}}. \tag{4.2}$$

Finally, the discrete scheme for single phase flow is completed by using Eq. (4.2) to define the closed integral of net (Gaussian) flux over the control volume (i, j), which results in

$$F_{i+1/2,j} - F_{i-1/2,j} + F_{i,j+1/2} - F_{i,j-1/2} = m. \tag{4.3}$$

Flux for Dual Variable Location

If permeability assumes a cellwise constant distribution and flow variables are defined with respect to cell vertices (Fig. 1), then flux and pressure continuity across a control volume interface is immediately satisfied since the control volume interfaces lie inside the cells of constant permeability. In addition, if we suppose flux and pressure continuity are imposed locally at each cell face, then the interior cell face flux contributions will cancel in the Gaussian integral over the net control volume. A brief summary of the dual variable location scheme follows below; details are presented in [3, 7, 16].

The position vector $\mathbf{r} = (x, y)$ assumes a cellwise bilinear variation, with each quadrilateral cell mapped to a unit cell. Since permeabilities are cellwise constant, evaluation of transform derivatives at the respective cell centers leads to general tensors $\mathbf{T}_{i+1/2,j+1/2}$ that are also cellwise constant, and consequently the pressure can also assume a cellwise bilinear variation with local derivatives

$$\Phi_{\tilde{\xi}} = (1-\tilde{\eta})\Delta_{\xi}\Phi_{i+1/2,j} + \tilde{\eta}\Delta_{\xi}\Phi_{i+1/2,j+1}, \qquad \Phi_{\tilde{\eta}} = (1-\tilde{\xi})\Delta_{\eta}\Phi_{i,j+1/2} + \tilde{\xi}\Delta_{\eta}\Phi_{i+1,j+1/2}, \tag{4.4}$$

where $\Phi_{i,j}$ is the discrete vertex pressure at (i, j) and $0 \le \tilde{\xi}, \tilde{\eta} \le 1$ are the local cell transform coordinates and $\Delta_{\xi}\Phi_{i+1/2,j} = \Phi_{i+1,j} - \Phi_{i,j}$, $\Delta_{\eta}\Phi_{i,j+1/2} = \Phi_{i,j+1} - \Phi_{i,j}$.

The four discrete directional cell fluxes of Eq. (4.1) are derived by integrating Eq. (3.4) between cell centers and edge midpoints corresponding to half cell intervals in the $(\tilde{\xi}, \tilde{\eta})$ coordinate system. For example the south flux F_S has an $\tilde{\eta}$ integration interval of $\delta\Omega_C = [0, 1/2]$. Replacing $(\tilde{\xi}, \tilde{\eta})$ in the integrands with *prescribed* constant values $(\bar{\xi}, \bar{\eta})$ yields a family of symmetric positive definite schemes [3], with, e.g., south flux

$$F_{S_{i+1/2,j+1/2}}(\Phi) = -\frac{1}{2}\left[T_{aa_{i+1/2,j+1/2}}((1-\bar{\eta})\Delta_{\xi}\Phi_{i+1/2,j} + \bar{\eta}\Delta_{\xi}\Phi_{i+1/2,j+1}) + T_{ab_{i+1/2,j+1/2}}\frac{(\Delta_{\eta}\Phi_{i,j+1/2} + \Delta_{\eta}\Phi_{i+1,j+1/2})}{2}\right], \tag{4.5}$$

and the general tensor coefficients given by Eq. (3.5) are now piecewise constant over each cell. A Galerkin scheme is obtained for $\bar{\xi} = \bar{\eta} = 1/3$. Further details and properties are given in [3, 7, 16].

Algebraic Flux Continuity for Control-Volume Distributed Schemes

When rock and flow variables are chosen to be control volume distributed (i.e., point distributed or cell centered; Fig. 2), the tensor permeability can be discontinuous across the control volume faces and flux continuity must be enforced. A family of algebraically flux continuous schemes for the two-dimensional full tensor equation Eq. (3.3) is defined in [4, 10] for either a point-distributed or cell-centered discretization and an equivalent scheme is given independently, in [11–13]. In summary, four auxiliary continuous control volume interface pressures $(\phi_N, \phi_S, \phi_E, \phi_W)$ are introduced per cell, allowing pressure to vary linearly over each subcell triangle (Fig. 2c). Piecewise constant fluxes are then calculated with respect to each subcell triangular basis function, and the flux continuity constraints

$$\begin{aligned}
-(T_{aa}\Phi_{\tilde{\xi}} + T_{ab}\Phi_{\tilde{\eta}})|_S^1 &= -(T_{aa}\Phi_{\tilde{\xi}} + T_{ab}\Phi_{\tilde{\eta}})|_S^2,\\
-(T_{aa}\Phi_{\tilde{\xi}} + T_{ab}\Phi_{\tilde{\eta}})|_N^3 &= -(T_{aa}\Phi_{\tilde{\xi}} + T_{ab}\Phi_{\tilde{\eta}})|_N^4,\\
-(T_{ab}\Phi_{\tilde{\xi}} + T_{bb}\Phi_{\tilde{\eta}})|_E^2 &= -(T_{ab}\Phi_{\tilde{\xi}} + T_{bb}\Phi_{\tilde{\eta}})|_E^3\\
-(T_{ab}\Phi_{\tilde{\xi}} + T_{bb}\Phi_{\tilde{\eta}})|_W^1 &= -(T_{ab}\Phi_{\tilde{\xi}} + T_{bb}\Phi_{\tilde{\eta}})|_W^4
\end{aligned} \tag{4.6}$$

define a linear system of equations for the four interface pressures in terms of the four locally numbered cell vertex pressures $(\Phi_1, \Phi_2, \Phi_3, \Phi_4)$, where $\Phi_{i,j} = \Phi_1$ and $\Gamma|_{\sigma}^{j}$ denotes interface flux Γ at quadrature location σ and state at volume j. The actual position of σ along each cell edge defines the family [10]. Thus each cell face pressure can be expressed as a linear combination of the cell vertex pressures and the four algebraically continuous normal fluxes take the form

$$F_{\sigma}(\Phi) = -\frac{1}{2}\sum_{L=1}^{4}\beta_L^{\sigma}\Phi_L, \qquad \sigma = (N, S, E, W), \tag{4.7}$$

where σ indicates the local normal flux location. A full description of the schemes together with the procedure for obtaining the β_L^{σ} coefficients is given in [10].

Consistent Flux Factorization

As in the case of dual location, each control volume face flux can also be expressed as a linear combination of cell edge potential differences with

$$F_\sigma(\Phi) = -\frac{1}{2}\left(\alpha_1^\sigma \Delta_\xi \Phi_{i+1/2,\,j} + \alpha_2^\sigma \Delta_\eta \Phi_{i+1,\,j+1/2} + \alpha_3^\sigma \Delta_\eta \Phi_{i,\,j+1/2} + \alpha_4^\sigma \Delta_\xi \Phi_{i+1/2,\,j+1}\right), \tag{4.8}$$

where the α_L^σ coefficients are determined by equating the respective coefficients of the cell vertex potentials in Eqs. (4.7) and (4.8), leading to

$$\begin{pmatrix} -1 & 0 & -1 & 0 \\ 1 & -1 & 0 & 0 \\ 0 & 1 & 0 & 1 \\ 0 & 0 & 1 & -1 \end{pmatrix} \begin{pmatrix} \alpha_1^\sigma \\ \alpha_2^\sigma \\ \alpha_3^\sigma \\ \alpha_4^\sigma \end{pmatrix} = \begin{pmatrix} \beta_1^\sigma \\ \beta_2^\sigma \\ \beta_3^\sigma \\ \beta_4^\sigma \end{pmatrix}. \tag{4.9}$$

Upon summation of the equations of (4.9),

$$\sum_{L=1}^{4} \beta_L^\sigma = 0, \tag{4.10}$$

which demonstrates that the system is linearly dependent due to the zero flux identity which holds for constant potential. As a consequence the α_L^σ are only defined up to an additive constant and therefore each normal flux can be written as a leading two-point flux associated with the corresponding adjacent cell edge together with cross terms. For example, with respect to edge $i+1/2,\ j$ and south flux (Fig. 2b), we can choose $\alpha_4^S = 0$ so that

$$F_{S_{i+1/2,\,j+1/2}}(\Phi) = -\frac{1}{2}\left(\alpha_1^S \Delta_\xi \Phi_{i+1/2,\,j} + \alpha_2^S \Delta_\eta \Phi_{i+1,\,j+1/2} + \alpha_3^S \Delta_\eta \Phi_{i,\,j+1/2}\right). \tag{4.11}$$

In the case of a diagonal tensor with cell face midpoint quadrature [10] each directional flux will reduce to the product of a coefficient (given by the harmonic mean of the local leading directional canonical tensor coefficients, e.g., $T_{aa}|_S = 2T_{aa}|_S^1 T_{aa}|_S^2/(T_{aa}|_S^1 + T_{aa}|_S^2)$) multiplying the local potential difference. Therefore consistency of flux in Eq. (4.11) demands that for zero cross-flow gradient (i.e., $\Delta_\eta \Phi_{i+1,\,j+1/2} = \Delta_\eta \Phi_{i,\,j+1/2} = 0$) α_1^S be equal to the harmonic coefficient. The geometry metric components of tensor $\boldsymbol{T}$ can either be calculated at each cell edge continuity point or be conveniently approximated by cell centered values. The consistent factorization for the particular scheme and quadrature point σ can be deduced directly from the algebraic system; using Eq. (4.9) it follows that

$$\alpha_1^S = -\left(\beta_1^S + \beta_4^S\right), \tag{4.12}$$

which holds for any control volume geometry. By expressing the cross-flow coefficients as

$$\alpha_2^S = (c^S + w^S)/2, \qquad \alpha_3^S = (c^S - w^S)/2 \tag{4.13}$$

using the identity $\Delta_\eta \Delta_\xi \Phi_{i+1/2,\,j+1/2} = \Delta_\xi \Delta_\eta \Phi_{i+1/2,\,j+1/2}$ and Eqs. (4.11), (4.13), the most general form of a consistent flux at S can be expressed as

$$\begin{aligned} F_{S_{i+1/2,\,j+1/2}}(\Phi) = -\frac{1}{2}\Bigg(&\alpha_1^S((1-\chi^S)\Delta_\xi \Phi_{i+1/2,\,j} + \chi^S \Delta_\xi \Phi_{i+1/2,\,j+1}) \\ &+ \frac{c^S}{2}(\Delta_\eta \Phi_{i+1,\,j+1/2} + \Delta_\eta \Phi_{i,\,j+1/2})\Bigg), \end{aligned} \tag{4.14}$$

where $\chi^S = w^S/2\alpha_1^S$. By flux consistency (and Eq. (4.13)), $c^S = (\alpha_2^S + \alpha_3^S)$ represents a directionally weighted mean approximation of the cross flow coefficient T_{ab}. Comparing Eqs. (4.5) and (4.14) it follows that the normal fluxes of the two formulations have an analogous discrete form, the difference being in the actual discrete approximation of the full tensor coefficients, where the control volume distributed scheme coefficients α_j^σ embody a full tensor generalization of the harmonic mean defined via Eq. (4.6), while the dual variable scheme has cellwise constant coefficients; cf. Eq. (4.5). A closely related formulation that brings the above two formulations together in a locally homogenized sense is presented in [16], and the relationship between the above two formulations is examined in [10] for spatially constant coefficients.

Fully Implicit Coupled Formulation

A fully implicit formulation [1, 5, 6] is employed to solve Eq. (2.1), which is approximated in the discrete locally conservative integral form (per phase P) by

$$\begin{aligned}\left(s_{P_{i,j}}^{n+1} - s_{P_{i,j}}^{n}\right)\tau_{i,j} + \Delta t\left(\lambda_P\left(s_{P_{i+1/2,j}}^{n+1}\right)F_{i+1/2,j}(\Phi^{n+1}) - \lambda_P\left(s_{P_{i-1/2,j}}^{n+1}\right)F_{i-1/2,j}(\Phi^{n+1})\right.\\ \left. + \lambda_P\left(s_{P_{i,j+1/2}}^{n+1}\right)F_{i,j+1/2}(\Phi^{n+1}) - \lambda_P\left(s_{P_{i,j-1/2}}^{n+1}\right)F_{i,j-1/2}(\Phi^{n+1})\right) = \Delta t M_{P_{i,j}},\end{aligned} \tag{4.15}$$

where τ_i is the control volume and $F_{i+1/2,j}$ is defined by Eq. (4.2). The oil phase saturation is eliminated via Eq. (2.2) and the system is solved simultaneously for (s_1, Φ). The hyperbolic flux contribution is upwinded according to the local wave direction, e.g. based on $\lambda_P(s_{P_{i+1/2,j}}^{n+1})F_{i+1/2,j}(\Phi^{n+1})$ across control volume face $(i+1/2,\ j)$ for a positive outward wave with respect to face $(i+1/2,\ j)$, $s_{P_{i+1/2,j}}^{n+1} = s_{P_{i,j}}^{n+1}$; otherwise $s_{P_{i+1/2,j}}^{n+1} = s_{P_{i+1,j}}^{n+1}$.

5. INCREASED SUPPORT AND LOSS OF M-MATRICES WITH FULL TENSOR APPROXIMATION

The above full tensor schemes enlarge the discrete matrix from five to nine row entries in 2-D (3-D full tensors generally increase the support of the scheme from 7 to 19 or 27 entries per row). In addition, a discrete *full* tensor matrix can lose diagonal dominance, as discussed below. Without loss of generality of the method, we shall focus on the pressure equation matrix in two dimensions and note that such a matrix arises directly within a sequentially implicit, IMPES, or single-phase system.

M-Matrix

A matrix with entries $a_{i,j}$ is an M-matrix if

$$\begin{aligned} &a_{i,i} > 0, && \forall\, i\\ &a_{i,j} \le 0, && \forall\, i,\ j,\ i \ne j\\ &\sum_j a_{i,j} \ge 0, && \forall\, i \end{aligned} \tag{5.1}$$

with strict inequality for at least one row and the matrix is irreducible [2, 24]. Referring to the matrix of Eq. (A1.2) resulting from the dual variable scheme—cf. Eq. (4.5)—the conditions of Eq. (5.1) can be shown to be satisfied [3, 10] if in each cell

$$\min(T_{aa},\, T_{bb}) \ge \bar{\eta}(T_{aa} + T_{ab}) \ge |T_{ab}| \tag{5.2}$$

and a Dirichlet boundary condition for pressure is applied at least at one point (ensuring strict inequality for one row). In this case the approximation inherits a discrete maximum principle. In addition it can be shown that Eq. (5.2) is precisely the condition for positive transmissibility [22].

However, the inequality of Eq. (5.2) is a sufficient condition for ellipticity and only includes the subset of elliptic full tensors where the magnitude of the cross-flow coefficient does not exceed the minimum diagonal tensor coefficient. Consequently nine-node approximations of the full tensor equation cannot yield M-matrices for all elliptic *full* tensors. However, the additional cross terms involving $\overline{\eta}$ in Eq. A1.2 serve to generate a family of nine-point schemes, even for a diagonal tensor, that enhance diagonal dominance of a full tensor scheme for any nonzero value of $\overline{\eta}$ (thus χ) above. Conversely if $\overline{\eta}=0$ the inequality of Eq. (5.2) is never satisfied for *any* full tensor.

Note that while the above approximations of the full tensor pressure equation are symmetric positive definite [3], they are also conditionally diagonally dominant, and when coupled with the nonsymmetric diagonally dominant upwind approximation for the essentially hyperbolic phase equations, the resulting enlarged block Jacobian bandwidth of the fully implicit full tensor system Eq. (4.15) is neither symmetric positive definite nor diagonally dominant, in contrast to the standard diagonal tensor fully implicit formulation, which maintains a smaller Jacobian bandwidth with an underlying diagonal dominance.

6. OPERATOR SPLITTING AND SPLITTING AT THE MATRIX LEVEL

In this section and Section 7, strategies for designing full tensor schemes that only rely on standard size matrix inversion (i.e., 5 row entries in 2-D, 7 in 3-D) are considered. The strategies hinge upon calculation of the additional terms at the old time or iterate level. This gives rise to the notion of a semi-implicit scheme, where "five-point" entries are implicit and the remainder are explicit.

Let the fully implicit nine-point discretization matrix be denoted by $A^{(9)}$ and the discrete solution by Φ_h such that

$$A^{(9)}\Phi_h = m. \tag{6.1}$$

We shall illustrate schemes in two dimensions (the principle extends to three dimensions directly) that involve decomposition of the matrix $A^{(9)}$ into a pentadiagonal matrix $A^{(5)}$ and a residual matrix $A^{(9-5)}$ where

$$A^{(9)} = A^{(5)} + A^{(9-5)} \tag{6.2}$$

and that give rise to semi-implicit schemes of the form

$$A^{(5)}\Phi^{n+1} + A^{(9-5)}\Phi^{n} = m. \tag{6.3}$$

Matrix Level Splitting

First we shall consider a scheme that is derived directly from splitting at the matrix level. Such a splitting involves calculating all terms belonging to the standard pentadiagonal form at time level $n+1$; while the remaining entries are calculated at time level n, the respective

split matrices are denoted symbolically by

$$A^{(5)} = \begin{pmatrix} 0 & A^{(9)}_{i,j+1} & 0 \\ A^{(9)}_{i-1,j} & A^{(9)}_{i,j} & A^{(9)}_{i+1,j} \\ 0 & A^{(9)}_{i,j-1} & 0 \end{pmatrix}, \tag{6.4a}$$

$$A^{(9-5)} = A^{(9)} - A^{(5)} = \begin{pmatrix} A^{(9)}_{i-1,j+1} & 0 & A^{(9)}_{i+1,j+1} \\ 0 & 0 & 0 \\ A^{(9)}_{i-1,j-1} & 0 & A^{(9)}_{i+1,j-1} \end{pmatrix}. \tag{6.4b}$$

Stability of Matrix Splitting with Discrete Discontinuous Coefficients

If the condition of Eq. (5.2) holds for all cells, then $A^{(9)}$is an M-matrix and Eq. (6.4) defines a regular splitting [24] of the matrix and thus the scheme of Eq. (6.3) is stable for general discrete coefficients. Therefore when $A^{(9)}$ is an M-matrix, the reduced matrix $A^{(5)}$ defines a robust preconditioner for inverting the full bandwidth matrix $A^{(9)}$ via successive iteration of Eq. (6.3) to convergence.

Loss of Discrete Stability

A corollary is that a nine-point diagonal tensor approximation enhances preconditioner stability when a full tensor is present; cf. Section 5. Conversely, the scheme defined by $\overline{\eta} = 0$ is unconditionally nondiagonally dominant for any full tensor since condition (5.2) is violated and $A^{(9)}$ is not an M-matrix. The splitting for this case is illustrated in Appendix A2 for the dual variable scheme defined above where the following are shown:

(a) For variable coefficients, depending on the definition of the discrete operator, the cross terms can add additional contributions to the standard five-point scheme coefficients which can either enhance or destroy diagonal dominance of the resulting pentadiagonal preconditioning matrix Eq. (6.4a), depending on the sign of the term in Eq. (A2.1). Thus while matrix level splitting ensures that all terms which contribute to the pentadiagonal are implicit, even the pentadiagonal matrix $A^{(5)}$ cannot be shown to be an M-matrix for general discrete coefficients.

If Eq. (6.3) is not iterated to convergence at each time step, then irrespective of whether $A^{(9)}$ is an M-matrix,

(b) the corresponding flux is nonconservative (Appendix A2);

(c) an O(1) error is introduced in velocity (Appendix A2).

By splitting at the flux level it is shown in Section 7 that semi-implicit schemes can be defined for evolutionary problems that avoid the additional iterations required by splitting at the matrix level, while maintaining local conservation, consistency, and stability of the formulation.

7. GENERAL SPLIT TENSOR FLUX

We shall now construct split schemes from the flux, since as shown above, loss of conservation and zero divergence will result from any semi-implicit matrix splitting that does not respect these properties at the flux level.

In Section 4 we demonstrated that all of the finite volume schemes presented, including those designed to maintain algebraic flux continuity, have fluxes that can be cast in the form of a leading two-point flux corresponding to the diagonal tensor component together with cross-flow terms; cf. Eq. (4.11). This observation is exploited below.

The flux is now split so as to generate a semi-implicit scheme that retains an implicit approximation of the diagonal tensor contribution and employs an explicit approximation of all flux cross-flow terms, thereby retaining standard diagonal tensor Jacobian inversion, and preserves existing simulator code design and efficiency. The splitting is illustrated for the "south" flux at S (Figs. 1b and 2b) and is defined by

$$F^{\mathsf{S}}_{S_{i+1/2,\,j+1/2}}(\Phi^{n+1},\,\Phi^{n}) = F^{2P}_{S_{i+1/2,\,j+1/2}}(\Phi^{n+1}) + F_{S_{i+1/2,\,j+1/2}}(\Phi^{n}) - F^{2P}_{S_{i+1/2,\,j+1/2}}(\Phi^{n}), \quad (7.1)$$

where superscripts S and $2P$ are used to denote the respective split flux and two-point flux. From the above scheme formulations it follows that the leading two-point flux can be expressed as

$$F^{2P}_{S_{i+1/2,\,j+1/2}}(\Phi^{n+1}) = -\frac{1}{2}\alpha_1^S \Delta\Phi^{n+1}_{i+1/2,\,j}, \quad (7.2)$$

where α_1^S is defined by Eq. (4.12) for a control volume distributed scheme, or for the dual variable formulation, by analogy between Eqs. (4.5) and (4.14), $a_1^S = T_{aa_{i+1/2,\,j+1/2}}$. The general split flux defines a new semi-implicit formulation composed of the leading two-point flux (Eq. (7.2)) approximated implicitly at the new $n+1$ time level, and a cross-flow flux

$$F_{S_{i+1/2,\,j+1/2}}(\Phi^{n}) - F^{2P}_{S_{i+1/2,\,j+1/2}}(\Phi^{n}) = \alpha_2^S \Delta_\eta \Phi^n_{i+1,\,j+1/2} + \alpha_3^S \Delta_\eta \Phi^n_{i,\,j+1/2}, \quad (7.3)$$

which is calculated explicitly at time level n and by (4.14), (7.3) yields

$$-\left[\frac{\alpha_1^S\left(-\chi^S \Delta_\xi \Phi^n_{i+1/2,\,j} + \chi^S \Delta_\xi \Phi^n_{i+1/2,\,j+1}\right)}{2} + c^S \frac{\left(\Delta_\eta \Phi^n_{i,\,j+1/2} + \Delta_\eta \Phi^n_{i+1,\,j+1/2}\right)}{4}\right]. \quad (7.4)$$

Fully Coupled Semi-implicit Split Formulation

For mixed systems of equations such as Eq. (2.1), the semi-implicit flux can be formulated for IMPES via deferred correction [7]. A sequentially implicit formulation is another possibility. Here we formulate the semi-implicit flux within a fully implicit formulation, which leads to a fully coupled scheme that is fully implicit in saturation and fully implicit with respect to diagonal tensor pressure terms and explicit with respect to cross-flow pressure differences. The discrete scheme for each phase P is now written as

$$\begin{aligned}\left(s^{n+1}_{P_{i,j}} - s^{n}_{P_{i,j}}\right)\tau_{i,j} + \Delta t\Big(&\lambda_P\left(s^{n+1}_{P_{i+1/2,\,j}}\right)F^{\mathsf{S}}_{i+1/2,\,j}(\Phi^{n+1},\,\Phi^{n}) - \lambda_P\left(s^{n+1}_{P_{i-1/2,\,j}}\right)F^{\mathsf{S}}_{i-1/2,\,j}(\Phi^{n+1},\,\Phi^{n})\\ &+ \lambda_P\left(s^{n+1}_{P_{i,\,j+1/2}}\right)F^{\mathsf{S}}_{i,\,j+1/2}(\Phi^{n+1},\,\Phi^{n}) - \lambda_P\left(s^{n+1}_{P_{i,\,j-1/2}}\right)F^{\mathsf{S}}_{i,\,j-1/2}(\Phi^{n+1},\,\Phi^{n})\Big) = \Delta t M_{P_{i,j}}\end{aligned} \quad (7.5)$$

and uses a spatially consistent split time level flux where, e.g.,

$$F^{\mathsf{S}}_{i+1/2,\,j}(\Phi^{n+1},\,\Phi^{n}) = F^{\mathsf{S}}_{N_{i+1/2,\,j-1/2}}(\Phi^{n+1},\,\Phi^{n}) + F^{\mathsf{S}}_{S_{i+1/2,\,j+1/2}}(\Phi^{n+1},\,\Phi^{n}), \quad (7.6)$$

and the "south" flux is given by Eq. (7.1) and the other local cell fluxes are defined in an analogous fashion. As with the conventional fully implicit system of Eq. (4.15) the oil saturation is eliminated and the block system is solved for (s_1, Φ). Note that the upwind split flux direction at $(i+1/2, j)$ is now evaluated using $\lambda(s^{n+1}_{P_{i+1/2,j}})F^{\mathsf{S}}_{i+1/2,j}(\Phi^{n+1}, \Phi^n)$. The new flux defined through Eq. (7.1) retains local conservation and for incompressible flow a divergence-free velocity field is also maintained (as shown below). The full tensor Jacobian band width is considerably reduced in size, from 9 to 5 row entries in 2-D, and from 19 or even 27 to 7 row entries in 3-D. In addition to a compact standard shape diagonal tensor Jacobian, an underlying diagonal dominance is recovered and thus the Jacobian to be inverted is also better conditioned, while the actual diagonal tensor coefficients are defined by consistent approximations to T_{aa}, T_{bb} of Eq. (3.5).

Local Conservation, Consistency, and Stability

Discrete properties of the split flux scheme are best illustrated with respect to the pressure equation. The split flux nine-point scheme leads to the matrix decomposition

$$A^{(9)} = M^{(5)} + X^{(9)}, \tag{7.7}$$

and with respect to Eq. (6.1) the splitting can be expressed as

$$M^{(5)}\Phi^{n+1} + X^{(9)}\Phi^n = m, \tag{7.8}$$

where

$$M^{(5)} = \begin{pmatrix} 0 & M^{(5)}_{i,j+1} & 0 \\ M^{(5)}_{i-1,j} & M^{(5)}_{i,j} & M^{(5)}_{i+1,j} \\ 0 & M^{(5)}_{i,j-1} & 0 \end{pmatrix} \tag{7.9}$$

is the net discrete diagonally dominant five-point operator matrix resulting from two-point flux contributions, while the cross-flow matrix $X^{(9)}$ is defined by

$$X^{(9)} = A^{(9)} - M^{(5)} = \begin{pmatrix} X^{(9)}_{i-1,j+1} & X^{(9)}_{i,j+1} & X^{(9)}_{i+1,j+1} \\ X^{(9)}_{i-1,j} & X^{(9)}_{i,j} & X^{(9)}_{i+1,j} \\ X^{(9)}_{i-1,j-1} & X^{(9)}_{i,j-1} & X^{(9)}_{i+1,j-1} \end{pmatrix}. \tag{7.10}$$

The above split formulation applies to both the control volume distributed and dual variable formulations. The dual variable formulation matrix coefficients of the diagonally dominant five-point operator $M^{(5)}$ and the full tensor nine-point operator $A^{(9)}$ are defined in Eqs. (A1.1) and (A1.2), respectively; cf. Appendix A1.

For any quadrature point other than $\overline{\eta} = 0$, the cross-flow matrix will generally involve nonzero entries for all nine nodes, while the M-matrix is unchanged. For spatially constant coefficients with $\overline{\eta} = 0$ the splittings of Eqs. (6.4) and (7.8) produce identical matrix factorizations for the pressure equation; however, even in this case there is still an important distinction in the semi-implicit time-split flux.

Locally Conservative Flux

Since the splitting is defined with respect to the flux, the same flux that is added to the control volume integral at (i, j) is subtracted from the control volume at $(i+1, j)$, which ensures local conservation, while the net discrete representation of divergence is defined by Eq. (7.8).

Error Due to Flux Splitting

The relative flux error introduced by the split flux approximation is defined by the difference between the fully implicit flux and the split flux acting on the exact solution $\Phi(r, t)$. For example, the relative error in flux normal to the control volume face at S (Fig. 2b) is defined by subtracting the split flux of Eq. (7.1) from the flux of Eq. (4.14) to yield

$$\begin{aligned} &F_{S_{i+1/2,j+1/2}}(\Phi(r, t+\Delta t)) - F^{\mathsf{S}}_{S_{i+1/2,j+1/2}}(\Phi(r, t+\Delta t), \Phi(r, t)) \\ &= -\left[\frac{\alpha_1^S(-\chi^S \Delta_\xi \delta\Phi_{i+1/2,j} + \chi^S \Delta_\xi \delta\Phi_{i+1/2,j+1})}{2} + c^S \frac{(\Delta_\eta \delta\Phi_{i,j+1/2} + \Delta_\eta \delta\Phi_{i+1,j+1/2})}{4}\right], \end{aligned} \tag{7.11}$$

where $\delta\Phi_{i,j} = \Phi(r_{i,j}, t+\Delta t) - \Phi(r_{i,j}, t)$. The discrete normal velocity error is defined by dividing the flux error by the size of the control volume face Δl. The leading error is due to the off-diagonal tensor coefficient, and dividing Eq. (7.11) by Δl and performing Taylor series expansions about S at time t yields

$$\begin{aligned} &V_S(\Phi(r, t+\Delta t)) - V_S^{\mathsf{S}}(\Phi(r, t+\Delta t), \Phi(r, t)) \\ &\quad = -\frac{c^S}{2}\frac{\partial^2\Phi}{\partial l \partial t}\Delta t - \frac{\alpha_1^S \chi^S}{2}\frac{\partial^3\Phi}{\partial n \partial l \partial t}\Delta n \Delta t + O(\Delta n^2, \Delta t^2), \end{aligned} \tag{7.12}$$

which demonstrates that the split flux velocity V^{S} is spatially consistent. The relative divergence discretization error due to the flux splitting scheme is given by the difference between the conventional and split discrete operators acting on the exact solution, viz.

$$\begin{aligned} &A^{(9)}\Phi(r, t+\Delta t) - M^{(5)}\Phi(r, t+\Delta t) - X^{(9)}\Phi(r, t) \\ &\quad = X^{(9)}(\Phi(r, t+\Delta t) - \Phi(r, t)) = \Delta t X^{(9)} \Delta\Phi/\Delta t; \end{aligned} \tag{7.13}$$

the leading divergence discretization error due to the time splitting of a full tensor scheme is therefore

$$X^{(9)}\Phi_t \Delta t \approx 2\Delta t T_{ab} \Phi_{\xi\eta t} \approx O(\Delta t). \tag{7.14}$$

Stability

An error equation for the relative discrete solution error can be derived by subtracting Eq. (7.8) from Eq. (6.1) and using Eq. (7.7) to yield

$$M^{(5)} e_h^{n+1} + X^{(9)} e_h^n = 0, \tag{7.15}$$

where the relative discrete solution error is defined by

$$e_h^n = \Phi_h - \Phi^n \tag{7.16}$$

and is the difference between the discrete solution satisfying Eq. (6.1) and the evolutionary solution defined via Eq. (7.8). Time stepping or iteration of the scheme of Eq. (7.8) is stable provided that the spectral radius is bounded by unity, e.g., [25], which follows if

$$\left\| \left(M^{(5)}\right)^{-1} X^{(9)} \right\|_\mu = \left\| I - \left(M^{(5)}\right)^{-1} A^{(9)} \right\|_\mu \le 1. \tag{7.17}$$

If flux splitting is regular or weakly regular then (7.17) holds [24, 25]. In particular, if $A^{(9)}$ is diagonally dominant then the Jacobi iteration is stable with

$$\left\| I - D^{-1} A^{(9)} \right\|_\infty \le 1.$$

where D is the diagonal of $A^{(9)}$. Since $(M^5)^{-1}$ is a better approximate inverse than D^{-1}, (7.17) ($\mu = \infty$) can be expected to hold if $A^{(9)}$ is diagonally dominant. However, the schemes presented here are conditionally diagonally dominant for $\bar{\eta} > 0$; cf. Eq. (5.2).

Stability in L_2

Here we consider the stability of the semi-implicit or iterative scheme of Eq. (7.8) in the L_2 norm and perform a von Neumann analysis for the case of constant coefficients. In this case both the dual variable and flux continuous schemes can be reduced to the same discrete form [10]—cf. Eq. (A1.2)—with constant coefficients. Thus the split flux operators are defined by

$$\begin{aligned} M^{(5)}\Phi^{n+1} &= -T_{aa}\left(\Phi^{n+1}_{i+1,j} - 2\Phi^{n+1}_{i,j} + \Phi^{n+1}_{i-1,j}\right) - T_{bb}\left(\Phi^{n+1}_{i,j+1} - 2\Phi^{n+1}_{i,j} + \Phi^{n+1}_{i,j-1}\right) \\ X^{(9)}\Phi^{n} &= T_{ab}\left(\Phi^{n}_{i+1,j+1} - \Phi^{n}_{i-1,j+1} - \left(\Phi^{n}_{i+1,j-1} - \Phi^{n}_{i-1,j-1}\right)\right)/2 \\ &\quad + \bar{T}\left(4\Phi^{n}_{i,j} - 2\left(\Phi^{n}_{i+1,j} + \Phi^{n}_{i-1,j} + \Phi^{n}_{i,j+1} + \Phi^{n}_{i,j-1}\right)\right. \\ &\quad \left. + \Phi^{n}_{i+1,j+1} + \Phi^{n}_{i-1,j+1} + \Phi^{n}_{i+1,j-1} + \Phi^{n}_{i-1,j-1}\right), \end{aligned} \tag{7.18}$$

where $\bar{T} = \bar{\eta}(T_{aa} + T_{bb})/2$ and the error equation Eq. (7.15) is rewritten as

$$M^{(5)} e_h^{r+1} = -X^{(9)} e_h^r. \tag{7.19}$$

Expanding the local error as a Fourier series with component $\lambda^r e^{i(k_1\xi + k_2\eta)}$, where $k_1 = 2\pi K_1$, $k_2 = 2\pi K_2$, and K_1, K_2 are the respective (ξ, η) transform space wave numbers, substitution in Eq. (7.18) yields

$$\begin{aligned} M^{(5)} e_h^{r+1} &= -2\lambda^{r+1} e^{i(k_1\xi + k_2\eta)} (T_{aa}(\cos(k_1 h) - 1) + T_{bb}(\cos(k_2 h) - 1)) \\ X^{(9)} e_h^{r} &= -\lambda^{r} e^{i(k_1\xi + k_2\eta)} (2T_{ab}\sin(k_1 h)\sin(k_2 h) - 4\bar{T}(\cos(k_1 h) - 1)(\cos(k_2 h) - 1)) \end{aligned} \tag{7.20}$$

and stability follows if $|\lambda^{r+1}/\lambda^r| \le 1$. After substitution of Eq. (7.20) in Eq. (7.19) the stability condition—cf. Eq. (7.17)—is satisfied if

$$\left| \frac{T_{ab}\sin(k_1 h)\sin(k_2 h) + 2\bar{T}(\cos(k_1 h) - 1)(\cos(k_2 h) - 1)}{(T_{aa}(\cos(k_1 h) - 1) + T_{bb}(\cos(k_2 h) - 1))} \right| \le 1. \tag{7.21}$$

Expanding in terms of half angles (where $\theta_1 = k_1 h/2$, $\theta_2 = k_2 h/2$) and rearranging, the inequalities resulting from Eq. (7.21) are certainly satisfied if

$$T_{aa}\tan^2(\theta_1) + T_{bb}\tan^2(\theta_2) \pm 2|T_{ab}|\tan(\theta_1)\tan(\theta_2) + ((T_{aa} + T_{bb}) \pm 4\bar{T})\tan^2(\theta_1)\tan^2(\theta_2) \geq 0 \tag{7.22}$$

and since $\bar{\eta} < 1/2$ the coefficient of $\tan^2(\theta_1)\tan^2(\theta_2)$ is non-negative. Thus omitting the latter term, the inequality of Eq. (7.22) is still satisfied provided that the quadratic discriminent is zero or negative, which requires that $T_{ab}^2 \leq T_{aa}T_{bb}$. Therefore the family of split schemes is unconditionally stable for constant elliptic coefficients.

Semi-implicit Time Marching or Iteration in Summary

For a standalone pressure equation Eq. (7.8) defines an iteration strategy with $M^{(5)}$ acting as an approximate inverse or preconditioner. If $A^{(9)}$ is an M-matrix and iteration to convergence is performed then either the preconditioner resulting from matrix splitting or flux splitting can be employed. For a time-dependent system such as an IMPES formulation, then as in [7], Eq. (7.8) can either be similarly iterated to a prescribed convergence tolerance per time step or be used directly as a split operator to update the system at each time step. Note all approaches are driven by a reduced bandwidth matrix.

However, since the above analysis has shown that the semi-implicit scheme is conservative and consistent (introducing an error $O(\Delta t)$), and stability is proven for constant coefficients, the semi-implicit split flux scheme can be expected to produce the most efficient method for any formulation, effectively replacing inversion of a conditionally diagonally dominant nine-point matrix by inversion of a symmetric positive definite classical five-point M-matrix (27 by seven-point matrix operator in 3-D), and if stability problems are encountered additional iterations can still be performed.

In this work the focal point is a fully implicit formulation; the semi-implicit operator has been incorporated into a standard fully implicit diagonal tensor formulation, extending, applicability to full tensors while retaining the same large time step capability and only requiring inversion of a standard 5-point *block* Jacobian rather than the much larger block bandwidth nondiagonally dominant Jacobian matrix resulting from a conventional fully implicit full tensor formulation.

8. SPLIT TENSOR FLUX ON AN UNSTRUCTURED GRID

Flux splitting can also be applied to triangular grids. While the flux split Jacobian is not reduced in size for pure triangulations, diagonal dominance is recovered due to the split time level approximation of pressure in the flux divergence operator. Once formulated for both quadrilateral and triangular cells the method can be applied to any unstructured grid type. Here the extension to triangular grids is outlined below. As before, focus is on cell vertex-based schemes, and both the dual variable and point-distributed schemes are considered.

Dual Variable

Assuming permeability is piecewise constant over each triangle (Fig. 3a), pressure can assume a linear variation over each triangle with

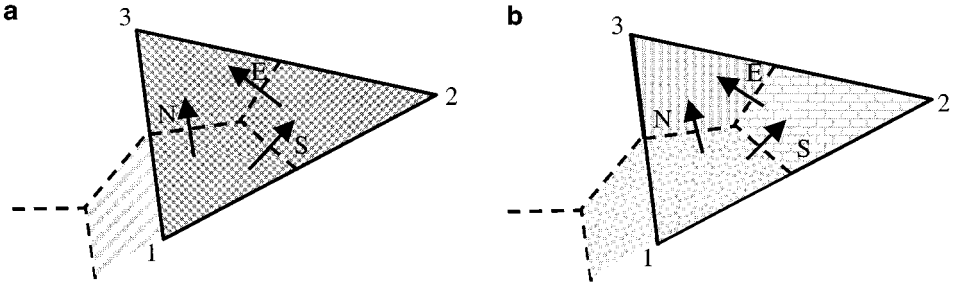

FIG. 3. Dual variable and control volume distributed schemes, fluxes for unstructured triangular grid. (a) Constant tensor per cell dual variable location. (b) Constant tensor per control volume, control volume distributed. Dashed line is a control volume face.

$$\Phi = \Phi_1 + \xi(\Phi_2 - \Phi_1) + \eta(\Phi_3 - \Phi_1) \tag{8.1}$$

and for example by Eq. (3.5), the outward normal flux approximation to the control volume face at (S) of Fig. 3a can be written as

$$F_S(\Phi) = -(T_{aa}(\Phi_2 - \Phi_1) + T_{ab}(\Phi_3 - \Phi_1)). \tag{8.2}$$

Point-Distributed

For the point-distributed scheme, pressure is vertex based and permeability is now piecewise constant over each control volume (Fig. 3b) and flux continuity must be enforced as before; cf. Eq. (4.6). In this case auxiliary pointwise continuous control volume face pressures are introduced at S, N, E, as indicated in Fig. 3b; cf. [6]. By analogy with Eq. (4.6), pressure can now assume a linear variation over the resulting subcell triangles, and normally resolved piecewise constant fluxes can be calculated at each control volume face. If we adopt notation analogous to that of Eq. (4.6), the flux continuity conditions at S, N, E lead to three equations for the unknown interface pressures,

$$\begin{aligned}
-(T_{aa}\Phi_{\tilde{\xi}} + T_{ab}\Phi_{\tilde{\eta}})|_S^1 &= -(T_{aa}\Phi_{\tilde{\xi}} + T_{ab}\Phi_{\tilde{\eta}})|_S^2 \\
-(T_{ab}\Phi_{\tilde{\xi}} + T_{bb}\Phi_{\tilde{\eta}})|_E^2 &= -(T_{ab}\Phi_{\tilde{\xi}} + T_{bb}\Phi_{\tilde{\eta}})|_E^3 \\
-(T_{ab}\Phi_{\tilde{\xi}} + T_{bb}\Phi_{\tilde{\eta}})|_N^1 &= -(T_{aa}\Phi_{\tilde{\xi}} + T_{ab}\Phi_{\tilde{\eta}})|_N^3,
\end{aligned} \tag{8.3}$$

enabling them to be expressed as a linear combination of the cell vertex pressures belonging to the triangle. Therefore each normal flux can then be expressed as

$$F_\sigma(\Phi) = -\frac{1}{2}\sum_{L=1}^{3} \beta_L^\sigma \Phi_L, \qquad \sigma = (S, N, E),$$

and as before (Eq. (4.10)), for a constant potential there is zero flux, thus $\sum_{L=1}^{3}\beta_L^\sigma = 0$, from which it follows that general form of the normal flux is

$$F_S(\Phi) = -\big(\alpha_1^S(\Phi_2 - \Phi_1) + \alpha_2^S(\Phi_3 - \Phi_1)\big), \tag{8.4}$$

where the coefficients ensure algebraic continuity; cf. Eq. (8.3). By consistency of normal flux, the coefficient α_1 will reduce to the harmonic mean of the local leading canonical

tensor coefficients with respect to the triangle control volume face, and α_2 is a directionally weighted average approximation of the cross-flow coefficient.

Thus as in the case of quadrilateral cells, each local control-volume normal flux can be expressed as the sum of a leading two-point flux (with coefficient α_1 above) together with a cross term. Therefore the split flux definition of Eq. (7.1) can be applied to both triangular formulations, and the resulting normal split flux at location S takes the form

$$F_S^{\mathrm{S}}(\Phi^{n+1}, \Phi^n) = -\big(\alpha_1^S\big(\Phi_2^{n+1} - \Phi_1^{n+1}\big) + \alpha_2^S\big(\Phi_3^n - \Phi_1^n\big)\big). \tag{8.5}$$

Finally the unstructured semi-implicit multiphase flow scheme can now be defined by

$$\big(s_{P_i}^{n+1} - s_{P_i}^n\big)\tau_i + \Delta t \sum_{k=1}^{N\text{edge}} \lambda_P\big(s_{P_{e(k,i)}}^{n+1}\big) F_{e(k,i)}^{\mathrm{S}}(\Phi^{n+1}, \Phi^n) = \Delta t M_{P_i},$$

where summation is over all edges $e(k, i)$ passing through the ith grid vertex, the net edge-based flux is composed of adjacent triangle and/or quadrilateral cell edge split fluxes according to each local grid cell type. As before, cell edge saturations are upwinded, the direction being a function of the local edge split flux.

9. RESULTS

The new full tensor split flux semi-implicit formulation is compared with the standard fully implicit diagonal and full tensor formulations. The water saturation field results are illustrated by contour plots ranging over 10 intervals and are displayed at time 0.5 pore volumes injected and no flow is assumed at all boundaries unless stated otherwise.

All solutions are computed with the semi-implicit split flux scheme, and generally large time steps are taken (average CFL of 12) while overall computation time is reduced when compared to a fully implicit full tensor formulation with a conventional full Jacobian inversion.

Case 1: Non-orthogonal Grid

In order to demonstrate grid effects, a nonorthogonal quadrilateral grid is employed for simulation of flow in a homogeneous isotropic reservoir, the grid is shown in Fig. 4a. An injector and producer are placed at the bottom left and top right hand corners of a square domain (quarter five-spot pattern). Nonorthogonality introduces a full tensor (cf. Eq. (3.5)). Standard simulators only allow diagonal tensor coefficients and include geometry effects by modifying these coefficients (called transmissibility modifiers, and multiply porosity by cell volume). The saturation field computed by a standard implicit scheme with diagonal tensor (corner-point) geometry, employing transmissibility modifiers, is shown in Fig. 4b. The reference solution, computed on a uniform 25×25 Cartesian grid, is shown in Fig. 4c and is symmetric about $y = x$. There is a large discrepancy between the results; due to the O(1) error in flux that is incurred when using the diagonal tensor on a nonorthogonal grid, the diagonal tensor approximation introduces a form of local grid orientation that causes the front to follow the curvature of the grid and leads to early breakthrough at the producing well. In contrast, the results from the full tensor schemes, using full matrix inversion (Fig. 4d) and using the split tensor operator (Fig. 4e), are in excellent agreement and compare favorably with the uniform grid result, demonstrating the need for a full tensor. The split flux operator reduces the difference in computation time between the full tensor (full matrix inverse) and diagonal tensor simulations by 60% for this case.

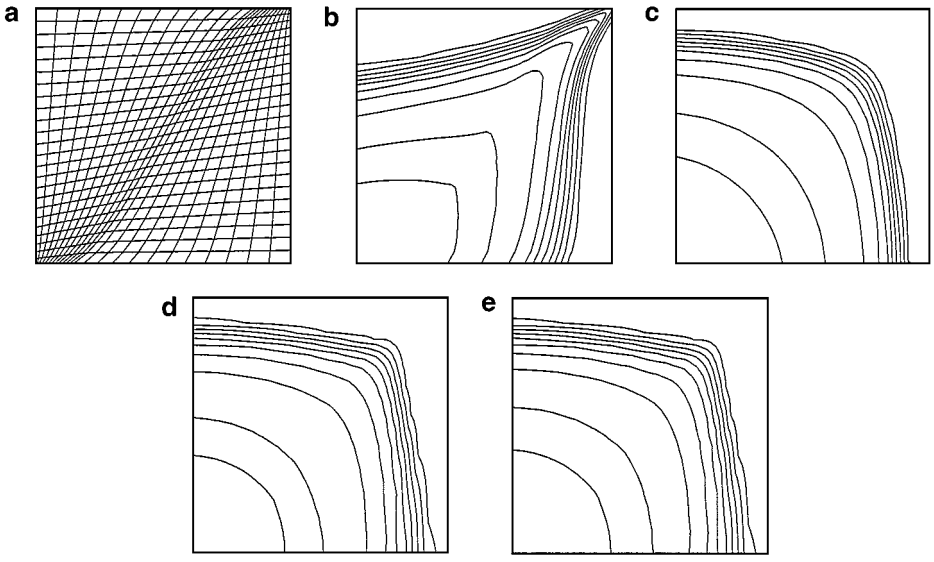

FIG. 4. Saturation contours and non-orthogonal grid. (a) Nonorthogonal grid. (b) Standard diagonal tensor saturation field on nonorthogonal grid. (c) Diagonal tensor saturation field on Cartesian grid. (d) Full tensor–full matrix saturation field. (e) Full tensor–split flux saturation field.

Case 2: Homogeneous Full Tensor

The second case involves an anisotropic diagonal homogeneous tensor with principal axes oriented at 45° to the reservoir domain. The dominant principal permeability direction is parallel to $y = x$, creating a full tensor with respect to the 30×30 Cartesian grid. The normalized full tensor has components $K_{aa} = 1,\ K_{bb} = 1,\ K_{ab} = 0.82$. Quarter five-spot boundary conditions are imposed as in Case 1. The results for this case are shown at time 0.4 pv. The standard diagonal tensor simulation omits cross terms and the saturation contours are shown in Fig. 5a. In contrast, the effect of the full tensor is shown in Fig 5b, the strong cross flow effect due to the dominant permeability that is parallel to the primary flow gradient is apparent from the elongated saturation front. Both of the full tensor schemes, using full matrix inversion (Fig. 5b) and using the split tensor operator (Fig. 5c), are again in excellent agreement, and the split scheme reduces the additional time required for full tensor simulation with full matrix inversion by nearly 86%.

A similar observation and saving is obtained for a principal axes orientation at $-45°$ to the reservoir domain, where now the primary flow gradient is orthogonal to the dominant permeability direction, causing a flattening of the front. Both of the full tensor schemes, using full matrix inversion (Fig. 5d), and using the split tensor operator (Fig. 5e), again sustain excellent agreement.

Case 3: Heterogeneous Cross Bed

This case involves an anisotropic heterogeneous domain with a 30% correlation length along the horizontal principal axis (Fig. 6a) and average anisotropy ratio of 10. The principal axes are oriented at 45° to the reservoir domain, and the dominant principal permeability direction is tangential to $y = x$, producing a heterogeneous full tensor permeability field with respect to the 30×30 Cartesian grid. Fluid is injected along the entire left-hand boundary

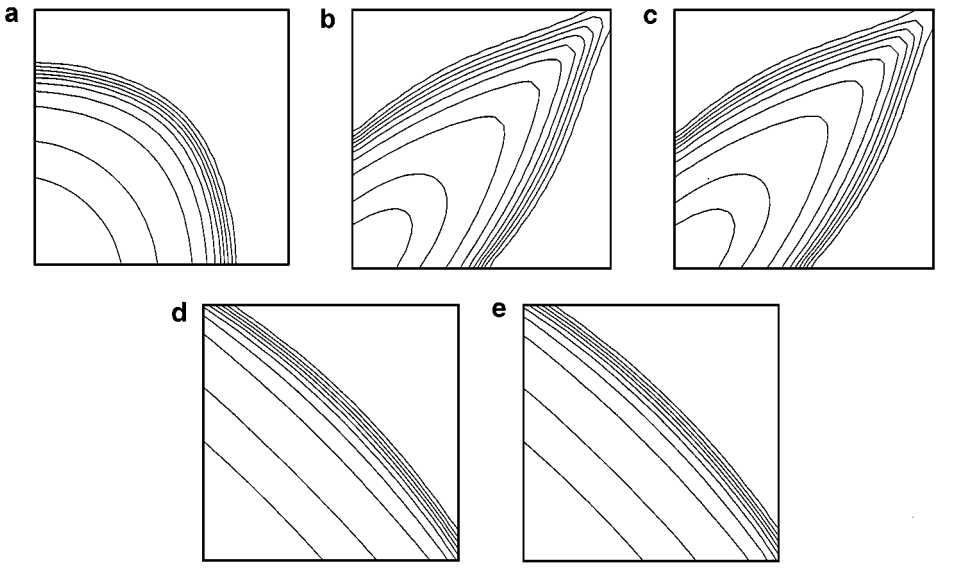

FIG. 5. Saturation contours for homogeneous full tensors. (a) Diagonal tensor coefficient saturation field. (b) Full tensor-full matrix. (c) Full tensor-split flux. (b, c) Principal axes max diagonal aligned with flow gradient. (d) Full tensor-full matrix. (e) Full tensor-split flux. (d, e) Principal axes max diagonal orthogonal to flow gradient.

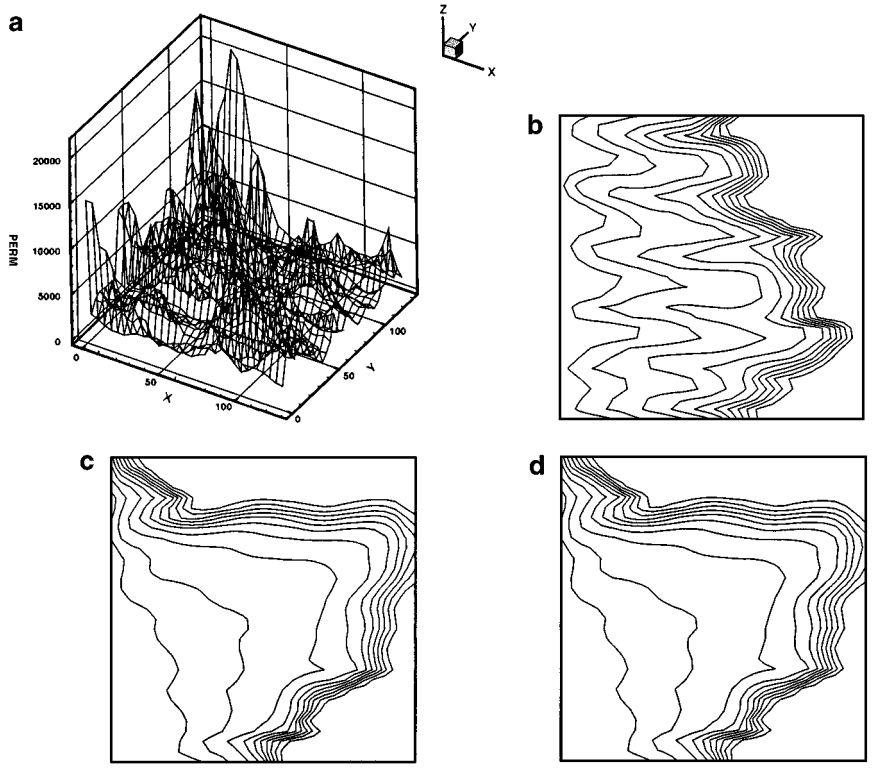

FIG. 6. Saturation contours and heterogeneous full tensor. (a) Permeability field. (b) Diagonal tensor coefficient saturation field. (c) Full tensor–full matrix saturation field. (d) Full tensor–split flux saturation field.

and produced at the right-hand boundary. Full tensor scheme results computed with full matrix inversion and using the split tensor operator are shown in Figs. 6c and 6d, respectively, and are in excellent agreement. The full tensor cross bed induces angled channeling of the front, demonstrating the influence of the underlying dominant principal tensor coefficient. The standard simulator diagonal tensor result (Fig. 6b) shows a completely different behavior, with channeling that is parallel to the horizontal and later breakthrough of the front at the completed producing well. This result further illustrates the effect of the O(1) error in flux incurred by commercial simulators when neglecting critical off-diagonal terms of the tensor (cf. Eq. (3.5)). The split tensor scheme reduces the additional computation time required by full tensor simulation by 45% for this case.

Case 4: Unstructured Grid, Cross Bed

This case also involves an anisotropic heterogeneous domain, with dominant principal direction parallel to $y = x$ and oriented at 45° relative to the grid, creating a cross-bedded region with a full heterogeneous tensor. Quarter five-spot boundary conditions are imposed as in Case 1. The grid is defined by an unstructured Delaunay triangulation of the domain, and a permeability tensor is assigned to each cell vertex control volume, i.e., point distributed (Fig. 7a). Results from the full tensor schemes computed with full matrix inversion and the split tensor operator are shown in Figs. 7c and 7d, respectively, and are in very good agreement. A comparison with the diagonal tensor result of Fig. 7b shows the strong effect of the cross flow induced by the dominant principal permeability direction, parallel to $y = x$. In this case the domain is entirely triangulated and is a worst case for the method since the

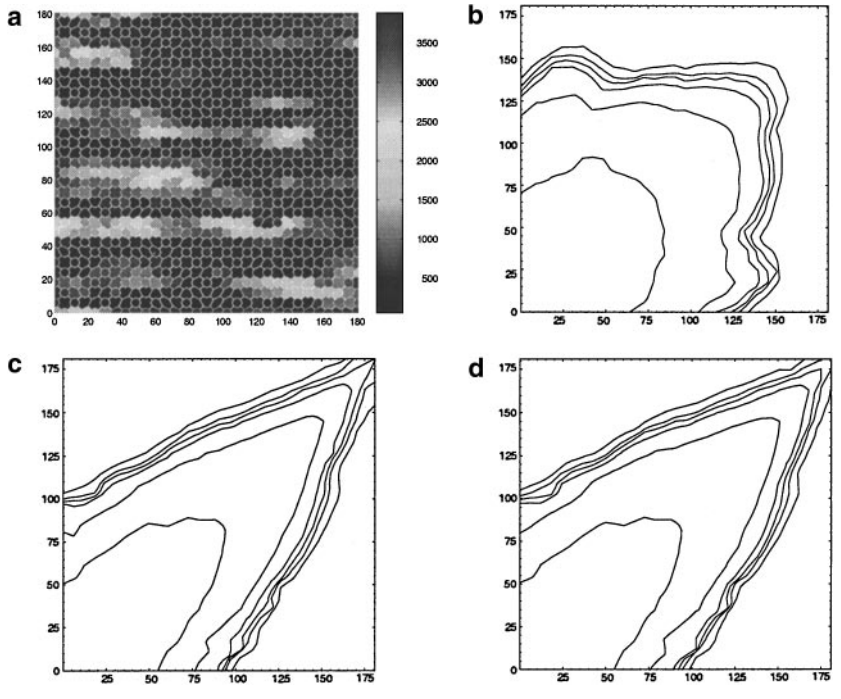

FIG. 7. Saturation contours, heterogeneous full tensor, and unstructured grid. (a) Permeability field and unstructured control volumes. (b) Diagonal tensor coefficient saturation field. (c) Full tensor–full matrix saturation field. (d) Full tensor–split flux saturation field.

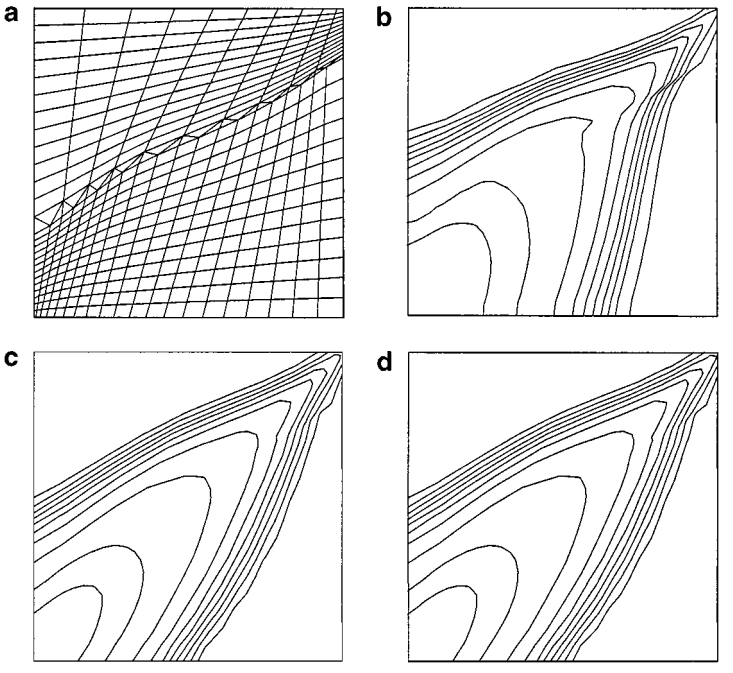

FIG. 8. Saturation contours and mixed cell unstructured grid. (a) Unstructured quadrilateral–triangular grid. (b) Diagonal tensor coefficient saturation field. (c) Full tensor–full matrix saturation field. (d) Full tensor–split flux saturation field.

split Jacobian is not reduced in size. However, improvement in efficiency is still obtained, with a reduction in additional full tensor computation time of 48%, which is attributed to the inherent diagonal dominance due to the split flux.

Case 5: Unstructured Quadrilateral Triangular Grid

The benefit of the completely general mixed cell scheme is illustrated by this example. The grid shown in Fig. 8a is composed of two quadrilateral domains 21×13 and 11×13 joined by a triangular interface, and is representative of local refinement, or a faulted region. The constant homogeneous full tensor of Case 2 is imposed on the domain and the problem is identical to Case 2 except for the use of an unstructured curvilinear grid instead of the Cartesian grid, which gives rise to an additional source of a full tensor.

Results are compared at the same output time as Case 2. The two-point flux scheme generates a highly distorted solution (Fig. 8b), due to the O(1) error in flux caused by neglecting the strong cross-flow terms. In addition to the generally incorrect shock front, the additional sensitivity due to the change in mesh type from quadrilateral to triangular is also clear in the solution.

In contrast, the results from the full tensor schemes, using full matrix inversion (Fig. 8c), and using the split tensor operator (Fig. 8d), are in excellent agreement and compare favorably with the uniform grid result of Figs. 5b and 5c, and show that the split operator can handle mixed element grids. The split flux operator reduces the difference in computation time between the full tensor (full matrix inverse) and diagonal tensor simulations by 87% for this case.

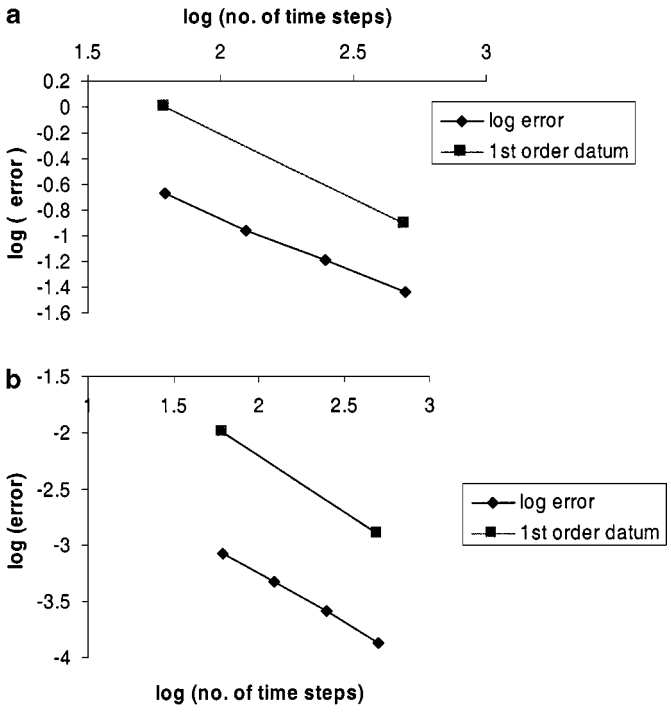

FIG. 9. Relative error convergence of saturation and pressure with decreasing time step. (a) L2 convergence of potential with decreasing time step. (b) L1 convergence of saturation with decreasing time step.

Relative Convergence

The full tensor discretization schemes employed here have been shown to provide convergent results under mesh refinement studies for problems with discontinuous coefficients [10]. The split flux scheme has been shown (cf. Section 7) to have a discretization error of $O(\Delta t)$ relative to a fully implicit full tensor flux. Results of a convergence study of relative error between the fully implicit scheme and the split scheme are presented in Fig. 9. The solutions for Case 2 above are recomputed (four times) by both schemes, the maximum time step is halved for each successive computation, and the differences in the conventional and split flux pressure and saturation fields are computed in the L_2 and L_1 norms, respectively. The charts of Fig. 9 indicate that the convergence rates are approximately $O(\Delta t)$, confirming the estimate of Eqs. (7.12) and (7.14), and that the split flux scheme is therefore consistent and convergent.

10. CONCLUSIONS

A time split full tensor flux operator is developed and incorporated into a standard fully implicit diagonal tensor formulation, extending applicability to full tensors on structured and unstructured grids.

Two full tensor finite volume formulations are considered: dual variable and (flux continuous) point-distributed. A relationship is established between the discrete forms in a locally homogenized sense, and it is shown that the directional (normal) flux of both formulations can be written as a leading two-point flux together with terms that approximate

Test Case No.	Fully Implicit Diagonal Tensor	Fully Implicit Full Tensor	Semi Implicit Split Flux
1	1	1.52	1.21
2	1	1.65	1.13
3	1	1.32	1.17
4	1	1.3	1.15
5	1	1.47	1.05

FIG. 10. Computation time: performance relative to fully implicit diagonal tensor simulation.

cross flow. This observation enables a general definition of split flux to be applied to both formulations.

The resulting time split full tensor flux operators enable any diagonal tensor formulation (from single phase to fully implicit) to be extended to a full tensor formulation while retaining diagonal tensor Jacobian inversion at each time step.

While operator splitting can also be defined at the matrix level, it is shown that when implemented as a semi-implicit scheme, flux splitting retains important discrete properties including local conservation and convergence that are lost by matrix splitting. It is shown that flux splitting is consistent and has a relative error of $O(\Delta t)$, which is confirmed by a convergence study (Fig. 10). The benefits of split tensor operators for multiphase flow are as follows:

(a) A spatially consistent full tensor flux is obtained while only requiring inversion of a diagonal tensor Jacobian, thus reducing computational requirements. For quadrilateral grids matrix entries reduce from nine to five per row in two dimensions.

(b) In addition to considerably reducing the size of the full tensor Jacobian bandwidth for quadrilateral grids, flux splitting ensures that the underlying diagonal dominance is recovered within the implicit operator block Jacobian for any formulation, on both structured and unstructured grids, in contrast to implicit full tensor Jacobian matrices, which have much larger bandwidths and are at best conditionally diagonally dominant.

(c) The pressure matrix to be inverted in the case of IMPES, sequentially implicit, and single-phase flow formulations is always a symmetric positive definite M-matrix for both structured and unstructured grids.

(d) Implementation of full tensor operators is simplified with all standard diagonal tensor Jacobian assembly remaining unchanged and entirely cell edge based for both structured and unstructured grids. Parallel Jacobian issues are also simplified.

(e) The split flux operator method produces results comparable to those of full matrix inversion, and both methods remove the O(1) error in flux that is introduced by the standard diagonal tensor formulation commonly employed in many existing simulators.

(f) The split operator method reduces the difference in computation time between full and diagonal tensor *fully implicit* simulations, usually by over 50% for cases tested, while retaining large (high CFL) time steps that are typical of fully implicit simulation.

(g) A Fourier stability analysis demonstrates unconditional stability of the semi-implicit family of schemes for a spatially constant elliptic full tensor.

(h) In 3-D much greater Jacobian reduction is obtained, for brick cells (19 to 7 or even 27 to 7) and further gains in efficiency are anticipated.

(i) The method is readily applicable to analogous mixed systems of partial differential equations such as the incompressible Euler and Navier–Stokes equations which also involve solving a pressure equation.

APPENDIX A1: MATRIX ENTRIES

The respective dual variable reduced five node M-matrix entries are given by

$$\begin{aligned}
M^{(5)}_{i+1,j} &= -\big(T_{aa_{i+1/2,j+1/2}} + T_{aa_{i+1/2,j-1/2}}\big)/2,\\
M^{(5)}_{i-1,j} &= -\big(T_{aa_{i-1/2,j+1/2}} + T_{aa_{i-1/2,j-1/2}}\big)/2\\
M^{(5)}_{i,j+1} &= -\big(T_{bb_{i+1/2,j+1/2}} + T_{bb_{i-1/2,j+1/2}}\big)/2,\\
M^{(5)}_{i,j-1} &= -\big(T_{bb_{i+1/2,j-1/2}} + T_{bb_{i-1/2,j-1/2}}\big)/2\\
M^{(5)}_{i,j} &= -\big(M^{(5)}_{i+1,j} + M^{(5)}_{i-1,j} + M^{(5)}_{i,j+1} + M^{(5)}_{i,j-1}\big)
\end{aligned} \tag{A1.1}$$

and the corresponding nine-node matrix is given by

$$\begin{aligned}
A^{(9)}_{i+1,j+1} &= -T_{ab_{i+1/2,j+1/2}}/2 - \frac{\eta}{2}\big(T_{aa_{i-1/2,j+1/2}} + T_{bb_{i+1/2,j+1/2}}\big)\\
A^{(9)}_{i-1,j-1} &= -T_{ab_{i-1/2,j-1/2}}/2 - \frac{\eta}{2}\big(T_{aa_{i-1/2,j-1/2}} + T_{bb_{i-1/2,j-1/2}}\big)\\
A^{(9)}_{i-1,j+1} &= T_{ab_{i-1/2,j+1/2}}/2 - \frac{\eta}{2}\big(T_{aa_{i-1/2,j+1/2}} + T_{bb_{i-1/2,j+1/2}}\big)\\
A^{(9)}_{i+1,j-1} &= T_{ab_{i+1/2,j-1/2}}/2 - \frac{\eta}{2}\big(T_{aa_{i+1/2,j-1/2}} + T_{bb_{i+1/2,j-1/2}}\big),
\end{aligned} \tag{A1.2a}$$

$$\begin{aligned}
A^{(9)}_{i+1,j} &= M^{(5)}_{i+1,j} + \frac{\eta}{2}\big(T_{aa_{i+1/2,j+1/2}} + T_{bb_{i+1/2,j+1/2}} + T_{aa_{i+1/2,j-1/2}} + T_{bb_{i+1/2,j-1/2}}\big)\\
A^{(9)}_{i-1,j} &= M^{(5)}_{i-1,j} + \frac{\eta}{2}\big(T_{aa_{i-1/2,j+1/2}} + T_{bb_{i-1/2,j+1/2}} + T_{aa_{i-1/2,j-1/2}} + T_{bb_{i-1/2,j-1/2}}\big)\\
A^{(9)}_{i,j+1} &= M^{(5)}_{i,j+1} + \frac{\eta}{2}\big(T_{aa_{i+1/2,j+1/2}} + T_{bb_{i+1/2,j+1/2}} + T_{aa_{i-1/2,j+1/2}} + T_{bb_{i-1/2,j+1/2}}\big)\\
A^{(9)}_{i,j-1} &= M^{(5)}_{i,j-1} + \frac{\eta}{2}\big(T_{aa_{i+1/2,j-1/2}} + T_{bb_{i+1/2,j-1/2}} + T_{aa_{i-1/2,j-1/2}} + T_{bb_{i-1/2,j-1/2}}\big),
\end{aligned} \tag{A1.2b}$$

and

$$\begin{aligned}
A^{(9)}_{i,j} = M^{(5)}_{i,j} &+ \frac{1}{2}\big(-T_{ab_{i+1/2,j+1/2}} - T_{ab_{i-1/2,j-1/2}} + T_{ab_{i-1/2,j+1/2}} + T_{ab_{i+1/2,j-1/2}}\big)\\
&- \frac{\eta}{2}\big(T_{aa_{i+1/2,j+1/2}} + T_{bb_{i+1/2,j+1/2}} + T_{aa_{i+1/2,j-1/2}} + T_{bb_{i+1/2,j-1/2}}\\
&+ T_{aa_{i-1/2,j+1/2}} + T_{bb_{i-1/2,j+1/2}} + T_{aa_{i-1/2,j-1/2}} + T_{bb_{i-1/2,j-1/2}}\big).
\end{aligned} \tag{A1.2c}$$

APPENDIX A2: MATRIX LEVEL SPLITTING

Loss of the Pentadiagonal M-Matrix

The splitting is illustrated for the simplest member scheme defined above with $\overline{\eta} = 0$. As can be seen from Eq. (A1.2), depending on the definition of the discrete operator, the cross terms can add additional contributions to the original five-point scheme coefficients. In this case for variable coefficients such that

$$\left(-T_{ab_{i+1/2,\,j+1/2}} - T_{ab_{i-1/2,\,j-1/2}} + T_{ab_{i-1/2,\,j+1/2}} + T_{ab_{i+1/2,\,j-1/2}}\right) \neq 0 \tag{A2.1}$$

an additional term is added to the diagonal, which can either enhance or destroy diagonal dominance of the resulting pentadiagonal matrix (Eq. (6.4a)) depending on the sign of the term in Eq. (A2.1). Thus while matrix level splitting ensures that all terms which contribute to the pentadiagonal are implicit, in general an M-matrix is not obtained.

Loss of Conservation Due to Matrix Splitting

The flux that is consistent with the above matrix splitting rule of Section 6 involves an implicit calculation of all terms that contribute to the five-point stencil at time level $n+1$, while other terms (cf. Eq. (6.4b)) are calculated explicitly at time level n. Again using the dual variable scheme for illustration, the matrix level splitting leads to the flux $\hat{F}$ at control volume face S of Fig. 2b, given by

$$\begin{aligned}\hat{F}_S(\Phi^{n+1}, \Phi^n) = -\Bigg[& T_{aa_{i+1/2,\,j+1/2}}\left((1-\overline{\eta})\left(\Phi^{n+1}_{i+1,\,j} - \Phi^{n+1}_{i,\,j}\right) + \overline{\eta}\left(\Phi^{n}_{i+1,\,j+1} - \Phi^{n+1}_{i,\,j}\right)\right) \\ & + T_{ab_{i+1/2,\,j+1/2}} \frac{\left(\left(\Phi^{n+1}_{i,\,j+1} - \Phi^{n+1}_{i,\,j}\right) + \left(\Phi^{n}_{i+1,\,j+1} - \Phi^{n+1}_{i+1,\,j}\right)\right)}{2} \Bigg] \frac{1}{2}.\end{aligned} \tag{A2.2}$$

However, by the same rule, for the equation at $i+1,\ j$, the flux corresponding to the same control-volume face 2 that is subtracted from the $i+1,\ j$ equation must take the form

$$\begin{aligned}\hat{F}_S(\Phi^{n+1}, \Phi^n) = -\Bigg[& T_{aa_{i+1/2,\,j+1/2}}\left((1-\overline{\eta})\left(\Phi^{n+1}_{i+1,\,j} - \Phi^{n+1}_{i,\,j}\right) + \overline{\eta}\left(\Phi^{n+1}_{i+1,\,j+1} - \Phi^{n}_{i,\,j}\right)\right) \\ & + T_{ab_{i+1/2,\,j+1/2}} \frac{\left(\left(\Phi^{n}_{i,\,j+1} - \Phi^{n+1}_{i,\,j}\right) + \left(\Phi^{n+1}_{i+1,\,j+1} - \Phi^{n+1}_{i+1,\,j}\right)\right)}{2} \Bigg] \frac{1}{2}.\end{aligned} \tag{A2.3}$$

and the net sum of outward normal fluxes with respect to $i,\ j$ forms the discrete split approximation of divergence defined by Eq. (6.3). However, it is clear that the fluxes of Eqs. (A2.2) and (A2.3) are unequal due to the differences in time level of the cross-flow contributions, and consequently local conservation is lost.

Error Due to Matrix Splitting

The leading error introduced in the normal flux by directly splitting the matrix is defined by subtracting the flux of Eq. (A2.2) from the flux of Eq. (4.14) with $F_S(\Phi^{n+1})$ to yield

$$F_S(\Phi^{n+1}) - \hat{F}_S(\Phi^{n+1}, \Phi^n) = -T_{ab_{i+1/2,\,j+1/2}} \frac{\delta\Phi_{i+1,\,j+1}}{4}, \tag{A2.4}$$

where $\delta\Phi_{i,j} = \Phi^{n+1}_{i,j} - \Phi^{n}_{i,j}$. The discrete normal velocity error is defined as before, dividing the flux error by the size of the control volume face Δl. The leading error is due to the off-diagonal tensor coefficient, and upon substitution of the exact solution in Eq. (A2.4), dividing by Δl and performing Taylor series expansions about S at time t

$$V_S(\Phi(r, t + \Delta t)) - \bar{V}_S(\Phi(r, t + \Delta t), \Phi(t)) = -T_{ab_{i+1/2,\,j+1/2}} \frac{\partial \Phi}{4\partial t} \frac{\Delta t}{\Delta l} \approx O(1). \quad \text{(A2.5)}$$

Therefore the semi-implicit velocity field will have an O(1) error. While for spatially constant coefficients the net error will cancel with respect to the divergence—cf. Eq. (6.3)—for multiphase flow, even this error will appear in the discrete local conservation law fluxes for the saturation equations.

ACKNOWLEDGMENTS

This research was funded by the Stanford University Industrial affiliates program (SUPRI-B) and Norsk Hydro.

REFERENCES

1. K. Aziz and A. Settari, *Petroleum Reservoir Simulation* (Applied Science, London, 1979).
2. P. Wesseling, *An Introduction to Multigrid Methods* (Wiley, New York, 1992).
3. M. G. Edwards, Symmetric, flux continuous, positive definite approximation of the elliptic full tensor pressure equation in local conservation form, in *13th SPE Reservoir Simulation Symposium, San Antonio, Tx, Feb. 1995*, p. 553.
4. M. G. Edwards and C. F. Rogers, A flux continuous scheme for the full tensor pressure equation, in *Proceedings: 4th European Conference on the Mathematics of Oil Recovery*, Norway, June 1994, edited by M. A. Christie, C. L. Farmer, O. Guillon, and Z. E. Heinemann.
5. S. Verma, *Flexible Grids for Reservoir Simulation*, Ph.D. thesis Stanford University, June 1996.
6. S. Verma and K. Aziz, A control volume scheme for flexible grids in reservoir simulation in *14th SPE Reservoir Simulation Symposium, Dallas, Texas, June 1997*, p. 215.
7. M. G. Edwards, Cross-flow, tensors and finite volume approximation with deferred correction, *Comput. Methods Appl. Mech. Engrg.* **151**, 143 (1998).
8. M. G. Edwards, Split elliptic tensor operators for reservoir simulation, in *Proceedings, ICFD Conference on Numerical Methods for Fluid Dynamics, Oxford University, Oxford, UK*, Mar./Apr. 1998.
9. L. J. Durlofsky, A triangle based mixed finite element—finite volume technique for modeling two phase flow through porous media, *J. Comput. Phys.* **105**, 252 (1993).
10. M. G. Edwards and C. F. Rogers, Finite volume discretization with imposed flux continuity for the general tensor pressure equation, *Comput. Geosci.* **2**, 259 (1998).
11. I. Aavatsmark, T. Barkve, O. Boe, and T. Mannseth, Discretization on non-orthogonal, curvilinear grids for multiphase flow, in *Proceedings: 4th European Conference on the Mathematics of Oil Recovery, Norway*, June 1994, edited by M. A. Christie, C. L. Farmer, O. Guillon, and Z. E. Heinemann.
12. I. Aavatsmark, T. Barkve, O. Boe, and T. Mannseth, Discretization on non-orthogonal, quadrilateral grids for inhomogeneous anisotropic media, *J. Comput. Phys.*
13. I. Aavatsmark, T. Barkve, and T. Mannseth, Control-volume discretization methods for 3D quadrilateral grids in inhomogeneous, anisotropic reservoirs, in *SPE Reservoir Simulation Symposium, Dallas, TX*, 1997.
14. T. Arbogast, M. F. Wheeler, and I. Yotov, Mixed finite elements for elliptic problems with tensor coefficients as cell centered finite differences, *SIAM Numer. Anal.* **34**(2), 828 (1997).
15. T. Arbogast, P. Keenan, M. F. Wheeler, and I. Yotov, Logically rectangular mixed methods for Darcy flow on general geometry, in *13th SPE Reservoir Simulation Symposium, San Antonio, TX*, Feb. 1995, p. 51.

16. M. G. Edwards, Superconvergent renormalization and tensor approximation, in *Proceedings: 5th European Conference on the Mathematics of Oil Recovery Loeben, Austria, Sept. 1996*, pp. 445–454, edited by Z. E. Heinemann.
17. S. H. Lee, L. J. Durlofsky, M. F. Lough, and W. Chen, Finite difference simulation of geologically complex reservoirs with tensor permeabilities, in *SPE Reservoir Simulation Symposium, Dallas, TX*, 1997.
18. C. L. Farmer, D. E. Heath, and R. O. Moody, A global optimization approach to grid generation, in *11th SPE Reservoir Simulation Symposium, Anaheim, CA, Feb. 1991*, p. 341.
19. J. Hyman, M. Shashkov, and S. Steinberg, The numerical solution of diffusion problems in strongly heterogeneous non-isotropic materials, *J. Comput. Phys.* **132**, 130 (1997).
20. P. I. Crumpton, G. Shaw, and A. Ware, Discretization and multigrid solution of mixed derivative terms and strongly discontinuous coefficients, *J. Comput. Phys.* **116**, 343 (1995).
21. L. J. Durlofsky, Numerical calculation of equivalent grid block permeability tensors for heterogeneous media, *Water Resources Res.* **27**, 699 (1991).
22. M. G. Edwards, "On the Relationship between M-Matrices and Positive Transmissibility", *in preparation*.
23. J. Bear, *Dynamics of Fluids in Porous Media* (American Elsevier, New York, 1972).
24. R. Varga, *Matrix Iterative Analysis* (Prentice Hall, New York, 1963).
25. W. Hackbusch, *Iterative Solution of Large Sparse Systems of Equations*, Applied Mathematical Sciences, Vol. 95 (Springer-Verlag, Berlin/New York, 1994).